

Synthesis, Structure, and Catalytic Performance in Cyclooctene Epoxidation of a Molybdenum Oxide/Bipyridine Hybrid Material: $\{[\text{MoO}_3(\text{bipy})][\text{MoO}_3(\text{H}_2\text{O})]\}_n$

Marta Abrantes,^{*,†,‡} Tatiana R. Amarante,[§] Margarida M. Antunes,[§] Sandra Gago,[§] Filipe A. Almeida Paz,[§] Irene Margiolaki,^{||} Alírio E. Rodrigues,[‡] Martyn Pillinger,[§] Anabela A. Valente,[§] and Isabel S. Gonçalves^{*,§}

[†]Centro de Química Estrutural, Complexo Interdisciplinar, Instituto Superior Técnico, Universidade Técnica de Lisboa, Av. Rovisco Pais, 1, 1049-001 Lisboa, Portugal, [‡]Laboratory of Separation and Reaction Engineering, Associate Laboratory LSRE/LCM, Faculdade de Engenharia da Universidade do Porto, Rua Dr. Roberto Frias, 4200-465, Porto, Portugal, [§]Department of Chemistry, CICECO, University of Aveiro, 3810-193 Aveiro, Portugal, and ^{||}European Synchrotron Radiation Facility, ESRF, BP-220, F-38043, Grenoble, France

Received March 12, 2010

The reaction of $[\text{MoO}_2\text{Cl}_2(\text{bipy})]$ (**1**) (bipy = 2,2'-bipyridine) with water in a Teflon-lined stainless steel autoclave (100 °C, 19 h), in an open reflux system with oil bath heating (12 h) or in a microwave synthesis system (120 °C, 4 h), gave the molybdenum oxide/bipyridine hybrid material $\{[\text{MoO}_3(\text{bipy})][\text{MoO}_3(\text{H}_2\text{O})]\}_n$ (**2**) as a microcrystalline powder in yields of 72–92%. The crystal structure of **2** determined from synchrotron X-ray powder diffraction data is composed of two distinct neutral one-dimensional polymers: an organic–inorganic polymer, $[\text{MoO}_3(\text{bipy})]_n$, and a purely inorganic chain, $[\text{MoO}_3(\text{H}_2\text{O})]_n$, which are interconnected by O–H...O hydrogen bonding interactions. Compound **2** is a moderately active, stable, and selective catalyst for the epoxidation of *cis*-cyclooctene at 55 °C with *tert*-butylhydroperoxide (*t*BuOOH, 5.5 M in decane or 70% aqueous) as the oxidant. Biphasic solid–liquid or triphasic solid–organic–aqueous mixtures are formed, and 1,2-epoxycyclooctane is the only reaction product. When *n*-hexane is employed as a cosolvent and *t*BuOOH(decane) is the oxidant, the catalytic reaction is heterogeneous in nature, and the solid catalyst can be recycled and reused without a loss of activity. For comparison, the catalytic performance of the precursor **1** was also investigated. The IR spectra of solids recovered after catalysis indicate that **1** transforms into the organic–inorganic polymer $[\text{MoO}_3(\text{bipy})]$ when the oxidant is *t*BuOOH(decane) and compound **2** when the oxidant is 70% aqueous *t*BuOOH.

Introduction

The chemistry of Mo^{VI} is very prominent in both industrial and biological systems. Several important industrial processes involving oxidation, ammoxidation, metathesis, and hydrocarbon dehydrogenation are carried out over Mo^{VI} catalysts.¹ Furthermore, as molybdenum is readily available to biological systems,² the coordination chemistry of Mo^{VI} has aroused considerable interest in view of its biochemical significance, and many Mo^{VI} complexes have been studied as models of molybdoenzymes.³

More specifically, Mo^{VI} complexes are very versatile catalysts for the liquid phase epoxidation of nonfunctionalized olefins in the presence of organic peroxides, as proven by the

Oxirane process.^{4,5} Since the chemistry of Mo^{VI} is largely dominated by complexes containing the *cis*-dioxomolybdenum(VI) structural unit,⁶ a very large number of these complexes have been investigated as epoxidation catalysts. Monomeric complexes^{7,8} of the type $[\text{MoO}_2\text{X}_m\text{L}_n]$ (X = mono/dianionic ligand, L = neutral ligand) and the related cationic derivatives⁹ $[\text{MoO}_2\text{X}_m\text{L}_n]^+[\text{Y}]^-$ have been shown to be active catalysts or catalyst precursors for homogeneous epoxidation of nonfunctionalized olefins, usually employing *tert*-butylhydroperoxide (*t*BuOOH) as the mono-oxygen source. Binuclear species of the type $[(\text{MoO}_2\text{X}_m\text{L}_n)_2\text{O}]$, which can be considered a special case of the monomeric species $[\text{MoO}_2\text{X}_m\text{L}_n]$ with X = $[\text{MoO}_3\text{X}_m\text{L}_n]^-$, have also proven to be active in the same catalytic reaction.^{8h,10} The motivation to study discrete, homogeneous catalysts in the form of monomeric or

*To whom correspondence should be addressed. Fax: +351 21 846 44 55 (M.A.), +351 234 370084 (I.S.G.). E-mail: marta.abrantes@ist.utl.pt (M.A.), igoncalves@ua.pt (I.S.G.).

(1) Chisole, G. P.; Maitlis, P. M. *Metal-catalysis in Industrial Organic Processes*; Royal Society of Chemistry Publishing: Cambridge, U. K., 2008.

(2) Hille, R. *Trends Biochem. Sci.* **2002**, *27*, 360.

(3) Enemark, J. H.; Cooney, J. J. A. *Chem. Rev.* **2004**, *104*, 1175.

(4) Comyns, A. E. *Encyclopedic dictionary of named processes in chemical technology*, 3rd ed.; Francis and Taylor: London, 2007.

(5) Jørgensen, K. A. *Chem. Rev.* **1989**, *89*, 431.

(6) For a recent review, see: Sanz, R.; Pedrosa, M. R. *Curr. Org. Synth.* **2009**, *6*, 239.

(7) For recent reviews, see: (a) Jeyakumar, K.; Chand, D. K. *J. Chem. Sci.* **2009**, *121*, 111. (b) Kühn, F. E.; Santos, A. M.; Abrantes, M. *Chem. Rev.* **2006**, *106*, 2455.

dimeric species stems from the fact that these are well-defined, single site catalysts, which usually favor high activities and selectivities. Furthermore, homogeneous molecular catalysts are amenable to precise modification as well as detailed mechanistic studies. However, the development of heterogeneous versions of homogeneous catalysts continues to be of paramount importance due to the potential benefits in catalyst separation and recycling, minimization of metal traces in the product, and improved handling and process control.¹¹ The challenge is to make a heterogeneous catalyst with the same catalytic properties and kinetics obtainable from the homogeneous counterpart.

One of the most successful methodologies for heterogenizing Mo^{VI} catalysts is to covalently anchor a functionalized derivative of the molecular catalyst onto an insoluble solid support of large surface area which can be either an organic polymer or an inorganic material.¹² Despite the advances made with these immobilized molecular catalysts, the conversion of dioxomolybdenum(VI) complexes into insoluble materials (for use as heterogeneous catalysts) without the need of an organic or inorganic support would be of immense interest. In 1997, Zubieta and co-workers described the synthesis of the hybrid material [MoO₃(bipy)] (bipy = 2,2'-bipyridine) in 10% yield by the hydrothermal treatment of a mixture of MoO₃, bipy, and water.¹³ Since the structure of

[MoO₃(bipy)] consists of one-dimensional chains of corner-sharing {MoO₄N₂} octahedra, it can be viewed as a polymeric version of [MoO₂(OR)₂(bipy)] complexes. Recently, we found that [MoO₃(bipy)] can be obtained rapidly and in quantitative yield by the oxidative decarbonylation of *cis*-[Mo(CO)₄(bipy)] with *t*BuOOH, paving the way to the catalytic application of this class of compounds.¹⁴ The organic–inorganic hybrid material was found to be an active, highly selective, and stable catalyst for the epoxidation of *cis*-cyclooctene with *t*BuOOH. Several other related monometallic molybdenum(VI) oxide based hybrid materials containing organonitrogen ligands directly coordinated to the oxide substructure have been described,¹⁵ but the catalytic potential of these systems has yet to be fully explored.

In the present paper, we report on the use of the complex [MoO₂Cl₂(bipy)] as a precursor to molybdenum(VI) oxide based hybrid materials. Specifically, the treatment of the dichloro complex with water under hydrothermal, open reflux, or microwave-assisted heating conditions gives good yields of a 1:1 adduct of two one-dimensional polymers, each formulated as [MoO₃(bipy)]_{*n*} and [MoO₃(H₂O)]_{*n*}. The chemistry and catalytic performance of the hybrid material in the epoxidation of *cis*-cyclooctene has been studied and compared with the behavior exhibited by the dichloro precursor.

Experimental Section

Materials and Methods. The monomer [MoO₂Cl₂(bipy)] (**1**) was synthesized according to the published procedure.^{8b} Elemental analysis was performed at the University of Aveiro. Atomic absorption spectroscopy (AAS) was performed at Instituto Superior Técnico using inductively coupled plasma optical emission spectroscopy (ICP-OES) after acid digestion of the sample. IR spectra were obtained using a FTIR Mattson-7000 infrared spectrophotometer. Attenuated total reflectance (ATR) spectra were measured on the same instrument equipped with a Specac Golden Gate Mk II ATR accessory having a diamond top-plate and KRS-5 focusing lenses. SEM with coupled EDS was carried out on a Hitachi SU-70 (S-4100) instrument using a 15 kV accelerating voltage. The microwave-assisted synthesis was carried out in a Discover S-class system, using a dynamic method in which the microwave power was automatically controlled on the basis of the temperature feedback measured using a vertical focused IR sensor.

{[MoO₃(bipy)][MoO₃(H₂O)]}_{*n*} (**2**). Three different heating methods were used to prepare **2**. For the hydrothermal method, a Teflon-lined stainless steel digestion bomb was charged with monomer **1** (1.67 g, 4.70 mmol) and water (50 mL) and heated for 19 h at 100 °C in an oven. For the reflux method, a mixture of **1** (0.22 g, 0.62 mmol) and water (30 mL) in a round bottomed flask was refluxed in the air (atmospheric pressure) for 12 h, using a thermostatted oil bath for heating. For the microwave-assisted method, a mixture of **1** (0.85 g, 2.39 mmol) and water (25 mL) was placed in a sealed glass reactor and heated at 120 °C

(8) (a) Kühn, F. E.; Lopes, A. D.; Santos, A. M.; Herdtweck, E.; Haider, J. J.; Romão, C. C.; Santos, A. G. *J. Mol. Catal. A: Chem.* **2000**, *151*, 147. (b) Kühn, F. E.; Groarke, M.; Bencze, É.; Herdtweck, E.; Prazeres, A.; Santos, A. M.; Calhorda, M. J.; Romão, C. C.; Gonçalves, I. S.; Lopes, A. D.; Pillinger, M. *Chem.—Eur. J.* **2002**, *8*, 2370. (c) Valente, A. A.; Moreira, J.; Lopes, A. D.; Pillinger, M.; Nunes, C. D.; Romão, C. C.; Kühn, F. E.; Gonçalves, I. S. *New J. Chem.* **2004**, *28*, 308. (d) Al-Ajlouni, A.; Valente, A. A.; Nunes, C. D.; Pillinger, M.; Santos, A. M.; Zhao, J.; Romão, C. C.; Gonçalves, I. S.; Kühn, F. E. *Eur. J. Inorg. Chem.* **2005**, 1716. (e) Veiros, L. F.; Prazeres, A.; Costa, P. J.; Romão, C. C.; Kühn, F. E.; Calhorda, M. J. *Dalton Trans.* **2006**, 1383. (f) Bruno, S. M.; Pereira, C. C. L.; Balula, M. S.; Nolasco, M.; Valente, A. A.; Hazell, A.; Pillinger, M.; Ribeiro-Claro, P.; Gonçalves, I. S. *J. Mol. Catal. A: Chem.* **2007**, *261*, 79. (g) Günyar, A.; Zhou, M.-D.; Drees, M.; Baxter, P. N. W.; Bassioni, G.; Herdtweck, E.; Kühn, F. E. *Dalton Trans.* **2009**, 8746. (h) Gago, S.; Neves, P.; Monteiro, B.; Pessêgo, M.; Lopes, A. D.; Valente, A. A.; Paz, F. A. A.; Pillinger, M.; Moreira, J.; Silva, C. M.; Gonçalves, I. S. *Eur. J. Inorg. Chem.* **2009**, 4528. (i) Wang, G.; Chen, G.; Luck, R. L.; Wang, Z.; Mu, Z.; Evans, D. G.; Duan, X. *Inorg. Chim. Acta* **2004**, *357*, 3223. (j) Jimtaisong, A.; Luck, R. L. *Inorg. Chem.* **2006**, *45*, 10391. (k) Feng, L.; Urnezis, E.; Luck, R. L. *J. Organomet. Chem.* **2008**, *693*, 1564.

(9) (a) Santos, A. M.; Kühn, F. E.; Bruus-Jensen, K.; Lucas, I.; Romão, C. C.; Herdtweck, E. *J. Chem. Soc., Dalton Trans.* **2001**, *8*, 1332. (b) Valente, A. A.; Petrovski, Ž.; Branco, L. C.; Afonso, C. A. M.; Pillinger, M.; Lopes, A. D.; Romão, C. C.; Nunes, C. D.; Gonçalves, I. S. *J. Mol. Catal. A: Chem.* **2004**, *218*, 5. (c) Petrovski, Ž.; Valente, A. A.; Pillinger, M.; Dias, A. S.; Rodrigues, S. S.; Romão, C. C.; Gonçalves, I. S. *J. Mol. Catal. A: Chem.* **2006**, *249*, 166. (d) Gago, S.; Balula, S. S.; Figueiredo, S.; Lopes, A. D.; Valente, A. A.; Pillinger, M.; Gonçalves, I. S. *Appl. Catal. A: Gen.* **2010**, *372*, 67.

(10) (a) Brito, J. A.; Gómez, M.; Muller, G.; Teruel, H.; Clinet, J.-C.; Duñach, E.; Maestro, M. A. *Eur. J. Inorg. Chem.* **2004**, 4278. (b) Martins, A. M.; Romão, C. C.; Abrantes, M.; Azevedo, M. C.; Cui, J.; Dias, A. R.; Duarte, M. T.; Lemos, M. A.; Lourenço, T.; Poli, R. *Organometallics* **2005**, *24*, 2582. (c) Pereira, C. C. L.; Balula, S. S.; Paz, F. A. A.; Valente, A. A.; Pillinger, M.; Klinowski, J.; Gonçalves, I. S. *Inorg. Chem.* **2007**, *46*, 8508. (d) Monteiro, B.; Gago, S.; Neves, P.; Valente, A. A.; Gonçalves, I. S.; Pereira, C. C. L.; Silva, C. M.; Pillinger, M. *Catal. Lett.* **2009**, *129*, 350.

(11) (a) Freund, C.; Herrmann, W. A.; Kühn, F. E. In *Topics in Organometallic Chemistry*; Springer-Verlag: Heidelberg, Germany, 2007; Vol. 22, p 39. (b) Heitbaum, M.; Glorius, F.; Escher, I. *Angew. Chem., Int. Ed.* **2006**, *45*, 4732.

(12) (a) For a recent review, see: Jain, K. R.; Kühn, F. E. *Dalton Trans.* **2008**, 2221. (b) Bruno, S. M.; Fernandes, J. A.; Martins, L. S.; Gonçalves, I. S.; Pillinger, M.; Ribeiro-Claro, P.; Rocha, J.; Valente, A. A. *Catal. Today* **2006**, *114*, 263 and references cited therein.

(13) Zapf, P. J.; Haushalter, R. C.; Zubieta, J. *Chem. Mater.* **1997**, *9*, 2019.

(14) Amarante, T. R.; Neves, P.; Coelho, A. C.; Gago, S.; Valente, A. A.; Paz, F. A. A.; Pillinger, M.; Gonçalves, I. S. *Organometallics* **2010**, *29*, 883.

(15) (a) Hagrman, P. J.; Hagrman, D.; Zubieta, J. *Angew. Chem., Int. Ed.* **1999**, *38*, 2639. (b) Zapf, P. J.; LaDuca, R. L., Jr.; Rarig, R. S., Jr.; Johnson, K. M., III; Zubieta, J. *Inorg. Chem.* **1998**, *37*, 3411. (c) Xu, Y.; Lu, J.; Goh, N. K. *J. Mater. Chem.* **1999**, *9*, 1599. (d) Hagrman, P. J.; LaDuca, R. L., Jr.; Koo, H.-J.; Rarig, R., Jr.; Haushalter, R. C.; Whangbo, M.-H.; Zubieta, J. *Inorg. Chem.* **2000**, *39*, 4311. (e) Zhou, Y.; Zhang, L.; Fun, H.-K.; You, X. *Inorg. Chem. Commun.* **2000**, *3*, 114. (f) Cui, C.-P.; Dai, J.-C.; Du, W.-X.; Fu, Z.-Y.; Hu, S.-M.; Wu, L.-M.; Wu, X.-T. *Polyhedron* **2002**, *21*, 175. (g) Lu, Y.; Wang, E.; Yuan, M.; Li, Y.; Hu, C. *J. Mol. Struct.* **2003**, *649*, 191. (h) Kim, J.; Lim, W. T.; Koo, B. K. *Inorg. Chim. Acta* **2007**, *360*, 2187. (i) Chuang, J.; Ouellette, W.; Zubieta, J. *Inorg. Chim. Acta* **2008**, *361*, 2357.

for 4 h. At the end of each reaction, a white solid suspended in a pale pink solution (pH 2–3) was obtained. After cooling to room temperature, the solid was recovered by centrifugation; washed with water, acetone, and diethyl ether; and dried at 100 °C. Yields were 72% (0.78 g), 91% (0.13 g), and 92% (0.51 g) for the hydrothermal, reflux, and microwave methods, respectively. Elemental analysis and FT-IR data were in agreement for all three methods; representative data are given here for the solid obtained using microwave-assisted heating. Anal. Calcd for $C_{10}H_{10}Mo_2N_2O_7$ (462.08): C, 25.99; H, 2.18; N, 6.06. Found: C, 25.85; H, 2.32; N, 6.04. No Cl was detected by EDS. Selected IR (KBr, cm^{-1}): 3224 m ($\nu(OH)$), 3121w, 3086w, 1679 m ($\delta(OH_2)$), 1608 m, 1600 m, 1575w, 1565w, 1496 m, 1475 m, 1444 m, 1315 m, 1248w, 1179w, 1159w, 1028 m, 1017 m, 955s ($\nu(O=Mo)$), 930s ($\nu(O=Mo)$), 916s ($\nu(O=Mo)$), 868s ($\nu(O=Mo)$), 757s, 682s,br ($\nu(Mo-O-Mo)$), 654 m, 636sh, 514s,br ($\nu(OMo_3)$), 439w, 415w, 400 m, 368w, 317w.

Synchrotron X-Ray Powder Diffraction Studies. High-resolution synchrotron X-ray powder diffraction (XRPD) data suitable for *ab initio* crystal solution were collected at 100 K using the powder diffractometer on beamline ID31 of the European Synchrotron Radiation Facility (ESRF), Grenoble, France.¹⁶ The beamline receives X-rays from the synchrotron source, operating with an average energy of 6 GeV and a beam current of typically 200 mA, from an undulator device. The high signal-to-noise ratio of the data is due to the high brilliance of the synchrotron beam in combination with a Si(111) crystal multianalyzer. The monochromatic wavelength was fixed at 0.29509(2) Å, calibrated against the Si standard NIST 640c [certified cell parameter $a = 5.4311946(92)$ Å]. Hard X-rays were selected for data collection of compound **2** to significantly reduce radiation damage, an occurrence observed in previous investigations using the same material but under different experimental conditions.

A finely powdered sample of **2** was placed inside a Hilgenberg borosilicate glass capillary with a diameter of *ca.* 0.4 mm, which was spun during data collection to improve powder averaging over the individual crystallites, ultimately removing any textural effects such as preferred orientation. Data were collected in continuous mode over an angular range of $0.519 \leq 2\theta \leq 20.001^\circ$, with accumulation times increasing with the scattering angle. The counts of the six detectors (covering roughly $5.5^\circ 2\theta$) were rebinned and normalized to give the equivalent step scans (0.003°) suitable for further structural analyses.

The collected high-resolution PXRD pattern of **2** was indexed by means of the routines provided with the software program DICVOL04,¹⁷ and by employing the first 20 well-resolved reflections (located using the derivative-based peak search algorithm provided with FullProf.2k¹⁸) and a fixed absolute error on each line of $0.03^\circ 2\theta$. Initial unit cell metrics were obtained with high figures of merit: $M(20)^{19} = 102.3$ and $F(20)^{20} = 224.9$; zero shift of $2\theta = -0.0053^\circ$.

(16) (a) Fitch, A. N. *The High Resolution Powder Diffraction Beam Line at ESRF in European Powder Diffraction: EPDIC IV, Pts 1 and 2*; Transtec Publications Ltd: Zurich-Uetikon, 1996; Vol. 228, p 219. (b) Fitch, A. N. *J. Res. Natl. Inst. Stand. Technol.* **2004**, *109*, 133.

(17) Boulouf, A.; Louer, D. *J. Appl. Crystallogr.* **2004**, *37*, 724.

(18) Rodriguez-Carvajal, J. FULLPROF: A Program for Rietveld Refinement and Pattern Matching Analysis. Abstract of the Satellite Meeting on Powder Diffraction of the XV Congress of the IUCR, Toulouse, France; 1990, 127. (b) Roisnel, T.; Rodriguez-Carvajal, J. *Mater. Sci. Forum* **2001**, *378–381*, 118; WinPLOTR [February 2008], A Windows Tool for Powder Diffraction Pattern Analysis, Proceedings of the Seventh European Powder Diffraction Conference (EPDIC 7).

(19) Boulouf, A.; Louer, D. *J. Appl. Crystallogr.* **1991**, *24*, 987.

(20) Louer, D. In *Automatic Indexing: Procedures and Applications, Accuracy in Powder Diffraction II*; NIST: Gaithersburg, MD, 1992; p 92.

(21) Laugier, J.; Bochu, B. *CHECKCELL, A Software Performing Automatic Cell/Space Group Determination*; Collaborative Computational Project Number 14 (CCP14), Laboratoire des Matériaux et du Génie Physique de l'Ecole Supérieure de Physique de Grenoble (INPG): Grenoble, France, 2000.

Evaluation of the systematic absences using CHECKCELL²¹ identified the monoclinic $P2_1/n$ space group as the most suitable. Structure solution was carried out using the direct methods of SIRPOW included in the software package EXPO2004 (version 2.1).²² After subtraction of the background using polynomial functions in selected angular intervals, the intensity of each individual reflection was extracted by employing Pearson profile functions. This strategy allowed the location of most non-hydrogen atoms composing the two neutral polymers, namely, all metal centers and oxygen atoms. Despite the high signal-to-noise ratio of the collected pattern, the location of the atoms comprising the coordinated 2,2'-bipyridine ligand was extremely difficult. Initial crystallographic positions were ultimately calculated in EXPO2004 by using a battery of heavy geometrical constraints for this chemical moiety.

Rietveld structural refinement²³ was performed with FullProf.2k¹⁸ by applying fixed background points throughout the entire angular range determined by the linear interpolation between consecutive (and manually selected) breakpoints in the powder pattern. Thompson–Cox–Hastings pseudo-Voigt (convoluted with axial divergency symmetry)²⁴ profile functions, along with two asymmetry correction parameters, were selected to generate the line shapes of the simulated diffraction peaks. This profile function produced markedly better fits than other more commonly employed functions such as pseudo-Voigt or split pseudo-Voigt functions. The angular dependence of the full-width-at-half-maximum of individual reflections was also taken into account by employing a Caglioti function correction.²⁵

Structural refinement using the atomic coordinates derived from EXPO2004 was done in consecutive stages to avoid refinement instability and divergence. Zero shift, scale factor parameters related to peak shape and unit cell parameters were consecutively added as fully refineable variables upon previous full convergence of the remaining parameters to their optimal values. Fractional atomic coordinates of all metal centers and oxygen atoms were ultimately allowed to refine freely. An overall common isotropic displacement parameter was added to the structural model as a fully refineable parameter. No correction was made for absorption effects.

After full convergence, the coordinates of the hydrogen atoms associated with the aromatic carbon atoms were generated using the appropriate *HFIX* routines implemented in SHELX,²⁶ and those belonging to the coordinated water molecule were calculated geometrically in order to provide the best geometrical fitting for the O–H···O hydrogen bonding interactions. All of these hydrogen atoms were added to the structural model and not allowed to refine. The same strategy was employed for all atoms composing the coordinated bipy molecule because, even with a battery of geometrical constraints, chemically feasible geometries for this moiety could not be achieved for unrestrained refinements. Thus, the location of this moiety in the final structural model does not arise as that which provides the best fit to the synchrotron data, hence the various small discrepancies observed for the Rietveld plot in Figure 1.

The oxidation states of the two crystallographically independent molybdenum centers were further investigated using PLATON,²⁷ with the valences of all of the Mo–O and Mo–N interactions being calculated from the measured bond distances

(22) Altomare, A.; Burla, M. C.; Camalli, M.; Carrozzini, B.; Casciaro, G. L.; Giacovazzo, C.; Guagliardi, A.; Moliterni, A. G. G.; Polidori, G.; Rizzi, R. *J. Appl. Crystallogr.* **1999**, *32*, 339.

(23) Rietveld, H. M. *J. Appl. Crystallogr.* **1969**, *2*, 65.

(24) Finger, L. W.; Cox, D. E.; Jephcoat, A. P. *J. Appl. Crystallogr.* **1994**, *27*, 892.

(25) Caglioti, G.; Paoletti, A.; Ricci, F. P. *Nucl. Instr.* **1958**, *3*, 223.

(26) Sheldrick, G. M. *SHELXL-97*; University of Göttingen: Göttingen, Germany, 1997.

(27) (a) Spek, A. L. *Acta Crystallogr., Sect. A: Found. Crystallogr.* **1990**, *46*, C34. (b) Spek, A. L. *J. Appl. Crystallogr.* **2003**, *36*, 7.

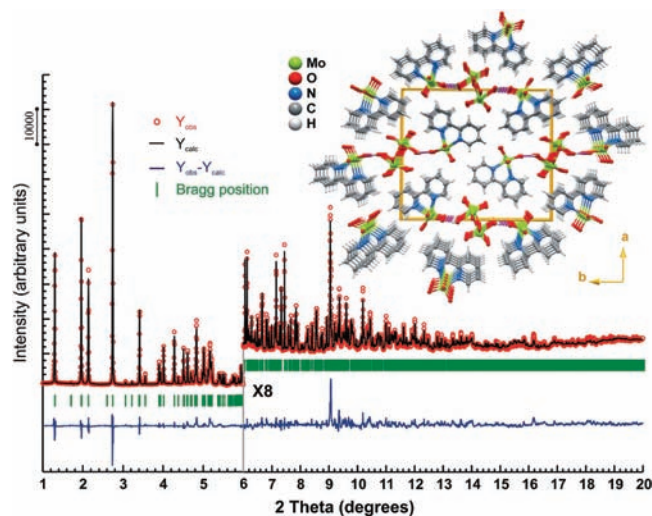


Figure 1. Final Rietveld plot (synchrotron XRPD data) of $\{[\text{MoO}_3(\text{bipy})][\text{MoO}_3(\text{H}_2\text{O})]\}_n$ (**2**). Observed data points are indicated as red circles; the best fit profile (upper trace) and the difference pattern (lower trace) are drawn as solid black and blue lines, respectively. Green vertical bars indicate the angular positions of the allowed Bragg reflections. Refinement details are given in Table 1. The inset shows a ball-and-stick crystal packing representation of **2** viewed along the [001] crystallographic direction.

following the theoretical models of Brese and O'Keefe²⁸ and Brown and Altermatt.²⁹ These studies allowed the unequivocal identification of the terminal oxygen atom of Mo(2) as belonging to a coordinated water molecule. The sums of the bond valences at each heavy atomic position are as follows (considering a +6 oxidation state for the molybdenum centers): Mo1 = +5.85 and Mo2 = +5.79. These results clearly suggest that the oxidation state of the two crystallographically independent metal centers composing each one of the polymers is indeed +6.

Table 1 gathers all of the details pertaining to the synchrotron X-ray data collection, crystal data, and structure refinement details for **2**. The corresponding final Rietveld plot is supplied in Figure 1.

Crystallographic data (excluding structure factors) for the structure reported in this paper have been deposited with the Cambridge Crystallographic Data Centre as supplementary publication number CCDC-755942. Copies of the data can be obtained free of charge upon application to CCDC, 12 Union Road, Cambridge CB2 2EZ, U.K. (Fax: (+44) 1223 336033. E-mail: deposit@ccdc.cam.ac.uk).

Catalytic Studies. The liquid-phase catalytic epoxidation reactions were carried out with magnetic stirring (800 rpm) at 55 °C under air (atmospheric pressure) in closed borosilicate reaction vessels (5 mL capacity) immersed in a thermostatted oil bath. Typically, the reaction vessel was loaded with **1** (0.018 mmol) or **2** (corresponding to 0.018 mmol $\{[\text{MoO}_3(\text{bipy})][\text{MoO}_3(\text{H}_2\text{O})]\}$), 1.8 mmol of *cis*-cyclooctene (Cy8), and 2.75 mmol of the oxidant (5.5 M *t*BuOOH in decane). The effect of adding 1,2-dichloroethane (DCE) or *n*-hexane (1 mL) as a cosolvent, or using 70% aqueous *t*BuOOH or 30% aqueous H₂O₂ instead of *t*BuOOH/decane, was investigated. After each reaction run of 48 h, the solid phase was recovered by centrifugation at 3500 rpm, washed with *n*-hexane, and dried at room temperature overnight. Subsequent 48 h runs using these solids were performed using olefin/oxidant/catalyst mass ratios identical to those used in the first run. The experiments designated as

Table 1. X-Ray Data Collection, Crystal Data, and Structure Refinement Details for $\{[\text{MoO}_3(\text{bipy})][\text{MoO}_3(\text{H}_2\text{O})]\}_n$ (**2**)

Data Collection	
diffractometer	ID31 at ESRF
wavelength/Å	0.29509(2)
temperature/K	100
geometry	Debye–Scherrer
2θ range (deg)	0.519 to 20.001
step size (deg)	0.003
Unit Cell	
formula	C ₁₀ H ₁₀ Mo ₂ N ₂ O ₇
fw	462.08
cryst syst	monoclinic
space group	<i>P</i> 2 ₁ / <i>n</i>
<i>a</i> /Å	17.32533(14)
<i>b</i> /Å	19.80459(16)
<i>c</i> /Å	3.75890(3)
γ/deg	95.5824(12)
<i>V</i> /Å ³	1283.642(18)
<i>Z</i>	4
<i>D</i> _c /g cm ⁻³	2.391
Profile Parameters	
profile function	Thompson–Cox–Hastings pseudo-Voigt
overall temperature factor	1.38(3) Å ²
Caglioti law parameters	<i>U</i> = 0.037(3) <i>V</i> = -0.0033(3) <i>W</i> = 0.00013(1)
asymmetry params (up to 5° 2θ)	0.0092(3) and 0.0034(1)
zero shift [2θ°]	0.0047(1)
Refinement Details	
no. of independent reflns	2257
no. of global refined params	1
no. of profile refined params	20
no. of intensity-dependent refined params	27
Reliability Factors for Data Points with Bragg Contribution (Conventional – Not Corrected for Background)	
<i>R</i> _p	7.11
<i>R</i> _{wp}	9.53
<i>R</i> _{exp}	2.21
χ ²	19.25
Structure Reliability Factors	
<i>R</i> _{Bragg}	12.0
<i>R</i> _F	15.8

CatFit were carried out for different solvent systems and involved performing the reaction of *cis*-cyclooctene (Cy8) with *t*BuOOH in decane at 55 °C in the presence of **2**, filtering off the solution after 1 h (at the reaction temperature) through a 0.2 μm PVDF w/GMF Whatman membrane and stirring the solution for a further 23 h at 55 °C. The aim of these experiments is to assess whether the catalytic reaction is homogeneous or heterogeneous in nature at the reaction temperature. A commonly used term for similar tests is “leaching test”, which aims to investigate the catalytic contribution of active species which are leached (desorbed) from a catalyst support into solution at the reaction temperature: hot filtration (with a careful choice of the material/pore size of the filter) of the solid catalyst is performed because physical adsorption is an exothermic process and therefore the cooling of the reaction mixture to room temperature may cause adsorption of metal species back onto the solid catalyst's surface. The term “leaching” may not be appropriate

(28) Brese, N. E.; O'Keefe, M. *Acta Crystallogr., Sect. B: Struct. Sci.* **1991**, *47*, 192.

(29) Brown, I. D.; Altermatt, D. *Acta Crystallogr., Sect. B: Struct. Sci.* **1985**, *41*, 244.

in the present work since, as discussed below, the homogeneous catalytic contribution is most likely due to enhanced catalyst solubility, rather than to the “leaching” of metal species.

The reaction courses were monitored using a Varian 3900 GC equipped with a capillary column (DB-5, 30 m × 0.25 mm) and a flame ionization detector.

Results and Discussion

Synthesis of $\{[\text{MoO}_3(\text{bipy})][\text{MoO}_3(\text{H}_2\text{O})]\}_n$ (2**).** As mentioned in the Introduction, the oxidative decarbonylation of *cis*- $[\text{Mo}(\text{CO})_4(\text{bipy})]$ with *t*BuOOH under mild conditions gives the one-dimensional organic–inorganic hybrid material $[\text{MoO}_3(\text{bipy})]$, which can be viewed as a polymeric version of $[\text{MoO}_2(\text{OR})_2(\text{bipy})]$ complexes.¹⁴ On the other hand, the same reaction with *cis*- $[\text{Mo}(\text{CO})_4(4,4'\text{-di-}t\text{-tert-butyl-2,2'\text{-bipyridine})]$ gives the discrete octameric complex $[\text{Mo}_8\text{O}_{24}(\text{di-}t\text{Bu-bipy})_4]$ instead of a polymeric material. This led us to investigate alternative soft chemistry routes to hybrid materials of the type $[\text{MoO}_3\text{L}_n]$, and in the present work, we describe our first attempt based on the hydrolysis and condensation of the monomeric complex $[\text{MoO}_2\text{Cl}_2(\text{bipy})]$ (**1**). To date, the chemistry of $[\text{MoO}_2\text{X}_m\text{L}_n]$ monomers in water has not been systematically investigated and has not been considered as a path to obtaining molybdenum(VI) oxide-based organic–inorganic hybrids. This is probably due to the general assumption that water is incompatible with this type of chemistry and would only promote an anarchic disruption of all of the metal–ligand bonds. However, the well-known sol–gel process used to synthesize stable metal oxide polymers and/or discrete metalloxanes relies precisely on the concept of controlled hydrolysis and condensation of reactive monomeric precursors.³⁰ Furthermore, several reports have shown that ligands of $[\text{MoO}_2\text{X}_m\text{L}_n]$ complexes may be partially resistant to protic environments.³¹ It is therefore surprising that the chemical reactivity of $[\text{MoO}_2\text{X}_m\text{L}_n]$ monomers in water has not yet been explored in a systematic way to obtain new compounds and more specifically molybdenum oxide-based hybrids.

The reaction of **1** with water was carried out either hydrothermally in a sealed Teflon-lined stainless steel digestion bomb (autogenous pressure, 100 °C, 19 h), in an open reflux system in the air (12 h, oil bath heating), or in a sealed glass vessel with microwave-assisted heating (120 °C, 4 h). In each case, a white solid suspended in an acidic solution (pH 2–3) was obtained, which was recovered by centrifugation, washed with water and organic solvents, and dried at 100 °C in the air. Practically identical elemental analysis, FT-IR, and X-ray powder diffraction data were obtained for all three solid products, indicating that the heating method had no significant influence on the outcome of the reaction. EDS analyses confirmed the absence of Cl in the products. On the basis of the characterization data and the crystal structure solution described below, the product is formulated as $\{[\text{MoO}_3(\text{bipy})][\text{MoO}_3(\text{H}_2\text{O})]\}_n$ (**2**) and is a 1:1 adduct of two one-dimensional polymers. The yields of **2** were 72% for the hydrothermal method and 91–92% for the microwave-assisted and reflux methods.

The FT-IR spectrum of **2** presents bands due to the coordinated bipy ligand (around 3100 cm^{-1} , in the range of 1610–1000 cm^{-1} and around 760 cm^{-1}), which are coincident with the bands observed for the monomer $[\text{MoO}_2\text{Cl}_2(\text{bipy})]$ (**1**)³² and for the known organic–inorganic hybrid compound $[\text{MoO}_3(\text{bipy})]$ (Figure 2).¹⁴ Furthermore, strong bands at 955, 930, 916, 868, 682, and 514 cm^{-1} , which may be assigned to Mo–O vibrations, are also present. For comparison, the polymer $[\text{MoO}_3(\text{bipy})]$ presents Mo–O vibrations at 914, 882, and 622 cm^{-1} . Taking into account the crystal structure of **2** (described below), the four bands at 955, 930, 916, and 868 cm^{-1} are attributed to Mo=O stretching vibrations from two distinct *cis*- $[\text{MoO}_2]^{2+}$ units. As expected, the bands in this region differ from the pair of Mo=O stretching vibrations exhibited by the precursor complex **1** (at 936 and 904 cm^{-1}).^{8b} The intense, broad bands at 682 and 514 cm^{-1} can be assigned to stretching vibrations of bridging Mo–O–Mo and OMo_3 units, respectively.³³ A very broad band around 3200 cm^{-1} and another at 1679 cm^{-1} indicate the presence of a water molecule.

Crystal Structure Description. Compound **2** was obtained as a microcrystalline powder, irrespective of the heating method used for the reaction of **1** in water. A complete elucidation of the crystal structure was only possible by employing *ab initio* methods based on high-resolution synchrotron XRPD data. The structure was ultimately formulated as $\{[\text{MoO}_3(\text{bipy})][\text{MoO}_3(\text{H}_2\text{O})]\}_n$ and is composed of two distinct neutral one-dimensional polymers: an organic–inorganic polymer, $[\text{MoO}_3(\text{bipy})]_n$, and a purely inorganic chain, $[\text{MoO}_3(\text{H}_2\text{O})]_n$, both based on Mo^{VI} metal centers, as unequivocally confirmed by bond valence calculations.

A search in the literature and in version 5.30 (November 2008 with four updates) of the Cambridge Structural Database (CDS)³⁴ shows that only a handful of related hybrid structures have been reported to date, namely those by the groups of Zhou, $[\text{Mo}_3\text{O}_9(1,10\text{-phenanthroline})_2]_n$,^{15c} Koo, $[(\text{Mo}_4\text{O}_{12})(\text{bipy})_3]_n$,^{15h} and Zubieta, $[\text{MoO}_3(\text{bipy})]_n$, $[\text{Mo}_2\text{O}_6(\text{bipy})]_n$, and $[\text{Mo}_3\text{O}_9(\text{bipy})]_n$.¹³ Compound **2** is, to the best of our knowledge, unprecedented. It differs from most of these previously reported structures in that the hybrid polymer is composed solely of one type of monomer, while in most of the aforementioned structures, $\{\text{MoO}_4\}$ tetrahedra periodically intercalate the monomers containing the organic ligand (either bipy or 1,10-phenanthroline). In contrast to the structure of $[\text{MoO}_3(\text{bipy})]_n$ reported by Zubieta and co-workers,¹³ which has all of the organic ligands distributed in such a way as to minimize steric repulsion between them, leading to a *pseudo*-star distribution, the hybrid polymer in **2** has all of the organic molecules perfectly aligned (i.e., eclipsed) in the direction of the growth of the polymer. Finally, **2** is remarkable because it is a 1:1 adduct of two one-dimensional polymers, in which one is a purely inorganic structure as described below.

(32) Šoptrajanov, B.; Trpkovska, M.; Pejov, L. *Croat. Chem. Acta* **1999**, *72*, 663.

(33) Seguin, L.; Figlarz, M.; Cavagnat, R.; Lassègues, J.-C. *Spectrochim. Acta Part A* **1995**, *51*, 1323.

(34) (a) Allen, F. H. *Acta Crystallogr., Sect. B: Struct. Sci.* **2002**, *58*, 380. (b) Allen, F. H.; Motherwell, W. D. S. *Acta Crystallogr., Sect. B: Struct. Sci.* **2002**, *58*, 407.

(30) Roesky, H. W.; Haiduc, I.; Hosmane, N. S. *Chem. Rev.* **2003**, *103*, 2579.

(31) Poli, R. *Coord. Chem. Rev.* **2008**, *252*, 1592.

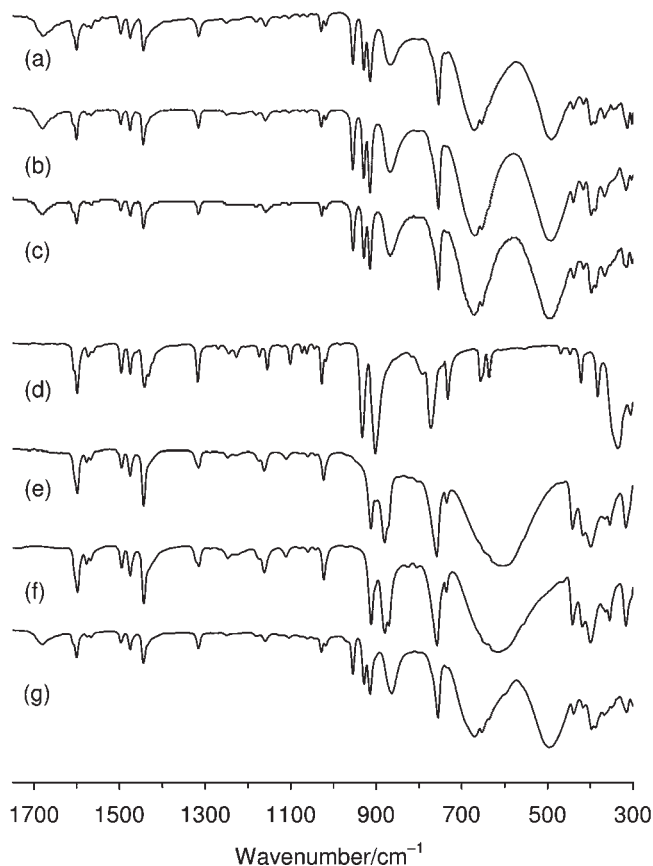


Figure 2. Comparison of the ATR FT-IR spectra of (a) $[\text{MoO}_3(\text{bipy})]_n$ (**2**), (d) $[\text{MoO}_2\text{Cl}_2(\text{bipy})]$ (**1**), and (e) $[\text{MoO}_3(\text{bipy})]$ with the spectra of the solids recovered after the first (run 1) or second (run 2) catalytic epoxidation runs: (b) **2**/*t*BuOOH(decane)/run2, (c) **2**/*t*BuOOH(aqueous)/run1, (f) **1**/*t*BuOOH(decane)/run2, and (g) **1**/*t*BuOOH(aqueous)/run1.

The crystallographically independent Mo(1) center in the one-dimensional organic–inorganic polymer $[\text{MoO}_3(\text{bipy})]_n$ (Figure 3a) is coordinated to two terminal oxo groups, one bipy organic molecule and two symmetry-related μ_2 -bridging oxo groups, with an overall $\{\text{MoN}_2\text{O}_4\}$ coordination geometry resembling a distorted octahedron as depicted in Figure 3b. The Mo–(N,O) distances range from 1.7829(14) to 2.3569(17) Å, and the internal (N,O)–Mo(1)–(N,O) *cis* and *trans* octahedral angles fall in the ranges of 76.83(6)–102.85(6)° and 160.27(6)–166.09(8)°, respectively (Table 2). The distortion of the Mo(1) coordination environment seems to arise from the combination of a significant *trans* effect of the Mo=O groups (which are *trans*-coordinated to the N-donor atoms of the organic moiety, see Figure 3b) and the distinct apical Mo–O distances of the μ_2 -bridges [1.6932(13) and 2.0933(13) Å]. Nevertheless, this hybrid polymer is characterized by only one intermetallic Mo···Mo distance of 3.759(1) Å.

The inorganic one-dimensional polymer $[\text{MoO}_3(\text{H}_2\text{O})]_n$ (Figure 4a) contains the other crystallographically independent Mo^{VI} center, Mo(2), which is coordinated to three μ_3 -bridging oxo groups, two terminal oxo groups, and one water molecule. The octahedral $\{\text{MoO}_6\}$ coordination environment (Figure 4b) is more distorted than that for Mo(1): the internal O–Mo(2)–O octahedral *trans* angles lie in the wide range of 139.67(7)–168.57(6)° and the *cis* angles are in the range of 68.57(5)–107.43(6)°. Nevertheless, the range found

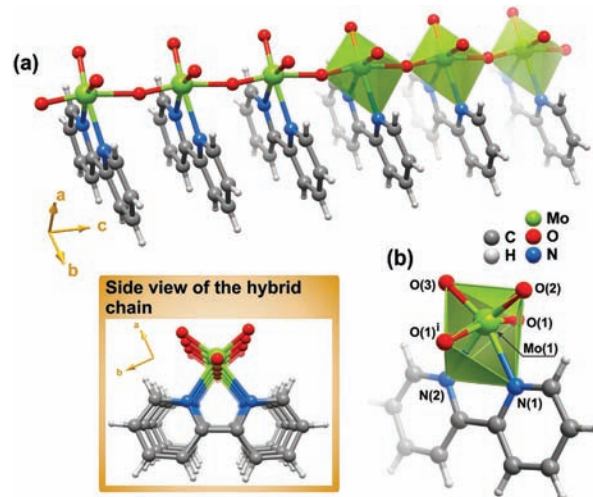


Figure 3. (a) Mixed ball-and-stick and polyhedral representations of the neutral $[\text{MoO}_3(\text{bipy})]_n$ hybrid polymer present in **2** running parallel to the [001] direction of the unit cell. (b) Schematic representation of the highly distorted $\{\text{MoN}_2\text{O}_4\}$ octahedral coordination geometry of Mo(1). Symmetry transformation used to generate equivalent atoms: (i) $x, y, -1 + z$.

Table 2. Selected Bond Lengths (Å) and Angles (deg) for the Two Molybdenum Coordination Environments Present in $[\{\text{MoO}_3(\text{bipy})\}[\text{MoO}_3(\text{H}_2\text{O})]_n$ (**2**)^a

Mo(1)–O(1)	1.6932(13)	Mo(2)–O(4)	1.9117(12)
Mo(1)–O(1) ⁱ	2.0933(13)	Mo(2)–O(4) ⁱⁱⁱ	2.0921(12)
Mo(1)–O(2)	1.7892(15)	Mo(2)–O(4) ^{iv}	2.2381(12)
Mo(1)–O(3)	1.7829(14)	Mo(2)–O(5) ⁱⁱ	1.7892(15)
Mo(1)–N(1)	2.2261(17)	Mo(2)–O(6)	1.7461(14)
Mo(1)–N(2)	2.3569(17)	Mo(2)–O(1W)	2.2506(15)
O(1)–Mo(1)–O(1) ⁱ	166.09(8)	O(4)–Mo(2)–O(4) ⁱⁱⁱ	139.67(7)
O(1)–Mo(1)–O(2)	95.20(6)	O(4)–Mo(2)–O(4) ^{iv}	68.57(5)
O(1)–Mo(1)–O(3)	97.03(6)	O(4)–Mo(2)–O(1W)	76.56(6)
O(1)–Mo(1)–N(1)	93.15(7)	O(4) ⁱⁱⁱ –Mo(2)–O(4) ^{iv}	74.32(5)
O(1) ⁱ –Mo(1)–N(1)	76.83(6)	O(4) ⁱⁱⁱ –Mo(2)–O(1W)	80.82(5)
O(1) ⁱ –Mo(1)–N(2)	78.35(5)	O(4) ^{iv} –Mo(2)–O(1W)	77.84(5)
O(1)–Mo(1)–N(2)	89.30(7)	O(5) ⁱⁱ –Mo(2)–O(4)	97.07(6)
O(2)–Mo(1)–N(1)	92.96(6)	O(5) ⁱⁱ –Mo(2)–O(4) ⁱⁱⁱ	98.86(6)
O(2)–Mo(1)–N(2)	163.29(6)	O(5) ⁱⁱ –Mo(2)–O(4) ^{iv}	91.04(6)
O(3)–Mo(1)–N(1)	160.27(6)	O(5) ⁱⁱ –Mo(2)–O(1W)	168.57(6)
O(2)–Mo(1)–O(1) ⁱ	94.94(6)	O(6)–Mo(2)–O(4)	107.43(6)
O(3)–Mo(1)–O(1) ⁱ	89.96(6)	O(6)–Mo(2)–O(4) ⁱⁱⁱ	103.03(5)
O(3)–Mo(1)–O(2)	102.85(6)	O(6)–Mo(2)–O(4) ^{iv}	162.26(6)
O(3)–Mo(1)–N(2)	92.52(6)	O(6)–Mo(2)–O(5) ⁱⁱ	106.67(7)
N(1)–Mo(1)–N(2)	70.69(6)	O(6)–Mo(2)–O(1W)	84.43(6)

^a Symmetry transformations used to generate equivalent atoms: (i) $x, y, -1 + z$; (ii) $x, 1 + y, z$; (iii) $x, y, 1 + z$; (iv) $1 - x, 2 - y, 1 - z$.

for the Mo–O bond distances [1.7461(14) to 2.2506(15) Å] is comparable with that found for the $\{\text{MoN}_2\text{O}_4\}$ coordination of Mo(1) (Table 2). The bond distance with the coordinated water molecule [2.2506(15) Å] is typical for dioxomolybdenum compounds, as revealed by a search in the CSD: for 33 entries, all Mo–O_{water} distances were found in the range of 2.20–2.44 Å with a median of 2.29 Å. Indeed, the possibility of the presence of a terminal hydroxyl group was discarded due to, on the one hand, bond valence calculations (described in detail in the Experimental Section) and, on the other, the fact that for the only known dioxomolybdenum compound with a terminal –OH group the bond distance to this moiety (*ca.* 1.97 Å) is significantly shorter than that registered for **2**.³⁵ The three symmetry-related O(4) atoms composing the $\{\text{MoO}_6\}$ coordination sphere, and structurally located in

(35) Isobe, M.; Marumo, F.; Yamase, T.; Ikawa, T. *Acta Crystallogr., Sect. B: Struct. Crystallogr. Cryst. Chem.* **1978**, *34*, 2728.

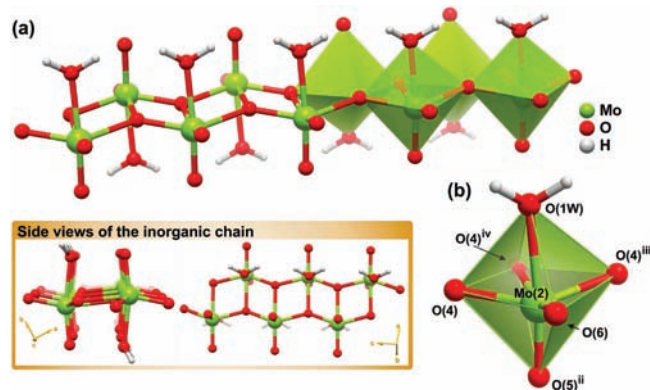


Figure 4. (a) Mixed ball-and-stick and polyhedral representations of the neutral $[\text{MoO}_3(\text{H}_2\text{O})]_n$ inorganic polymer present in **2** and running parallel to the [001] direction of the unit cell. (b) Schematic representation of the highly distorted $\{\text{MoO}_6\}$ octahedral coordination geometry of Mo(2). Symmetry transformations used to generate equivalent atoms: (ii) $x, 1 + y, z$; (iii) $x, y, 1 + z$; (iv) $1 - x, 2 - y, 1 - z$.

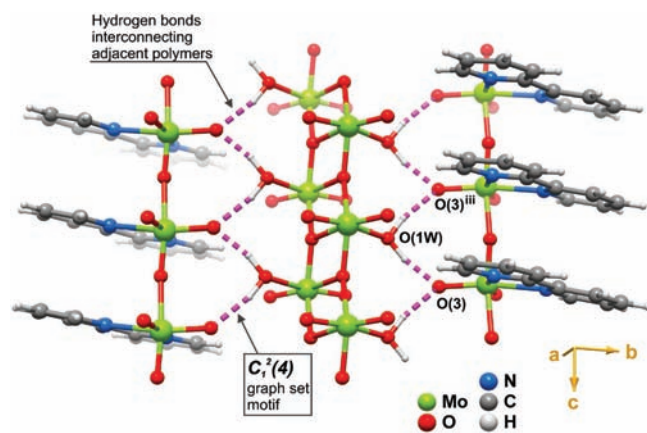


Figure 5. O–H···O hydrogen bonding interactions (dashed pink lines) interconnecting adjacent inorganic, $[\text{MoO}_3(\text{H}_2\text{O})]_n$, and hybrid, $[\text{MoO}_3(\text{bipy})]_n$, polymers in **2**, describing a $C_1^2(4)$ graph set motif running parallel to the [001] direction of the unit cell. For geometrical details of the represented hydrogen bonding interactions, see Table 3. Symmetry transformation used to generate equivalent atoms: (iii) $x, y, 1 + z$.

the equatorial plane of the octahedron, act as the μ_3 -bridges leading to the formation of an inorganic tape with all Mo^{VI} centers distributed in a zigzag fashion along the [001] direction. This arrangement leads to a slightly asymmetric distribution of intermetallic $\text{Mo}\cdots\text{Mo}$ distances along the chain: 3.434(1) and 3.452(1) Å.

The two polymers in **2** are linked by O–H···O hydrogen bonding interactions in which the coordinated water molecule of $[\text{MoO}_3(\text{H}_2\text{O})]_n$ donates the two hydrogen atoms to neighboring O(3) atoms of the terminal $\text{Mo}=\text{O}$ oxo groups of the adjacent $[\text{MoO}_3(\text{bipy})]_n$ polymer (Figure 5). These interactions are strong [$d_{\text{D}\cdots\text{A}}$ ranging between *ca.* 2.62 and 2.80 Å, Table 3] and highly directional. The recursive and cooperative fashion in which these interactions create supramolecular bridges along the [001] direction between the polymers leads ultimately to a $C_1^2(4)$ graph set motif³⁶ running parallel to the *c* axis. This arrangement produces a new supramolecular entity composed of two hybrid polymers and one inorganic

Table 3. Geometrical Details (distances in Å and angles in deg) of the Hydrogen Bonds Present in $\{[\text{MoO}_3(\text{bipy})][\text{MoO}_3(\text{H}_2\text{O})]_n\}$ (**2**)^a

D–H···A	$d(\text{D}\cdots\text{A})$	$\angle(\text{DHA})$
O(1W)–H(1B)···O(3)	2.6166(19)	167(2)
O(1W)–H(1C)···O(3) ⁱⁱⁱ	2.7959(19)	168(2)

^a Symmetry transformation used to generate equivalent atoms: (iii) $x, y, 1 + z$.

chain (Figure 5), which packs close in the *ab* plane of the unit cell in a brickwall-like fashion to yield the crystal structure of **2** (inset in Figure 1). The closest intermetallic $\text{Mo}\cdots\text{Mo}$ distance across polymers within this new entity is 5.811(1) Å.

Catalysis. The catalytic performance of **2** for olefin epoxidation was investigated using *cis*-cyclooctene (Cy8) as a model substrate, *t*BuOOH (5.5 M in decane) as an oxidant, and a reaction temperature of 55 °C. A catalyst/substrate/oxidant molar ratio of 1:100:150 was used. Irrespective of whether or not a cosolvent (*n*-hexane or 1,2-dichloroethane (DCE)) was used, biphasic solid–liquid mixtures were formed, and 1,2-epoxycyclooctane was the only product of Cy8 oxidation. The epoxide yields at 48 h were 34% (*n*-hexane), 49% (no cosolvent), and 62% (DCE), which are all higher than those obtained in the absence of a molybdenum-containing catalyst (19%, 11%, and 11%, respectively; Figure 6). These results indicate that **2** contains active metal species for olefin epoxidation. In our previous work, the one-dimensional organic–inorganic polymer $[\text{MoO}_3(\text{bipy})]$ was tested as a catalyst for Cy8 epoxidation under identical reaction conditions to those used in the present work (with DCE as a cosolvent).¹⁴ The Cy8 conversion at 24 h for compound **2** (45%) is notably lower than that registered for $[\text{MoO}_3(\text{bipy})]$ (81%). For comparison, the catalytic performance of the precursor **1** (without cosolvent) was investigated, and the results are shown in Figure 6. In the first run, the epoxide was formed as the only reaction product in yields of 78%/87% at 24 h/48 h, which are higher than those observed for **2** (34%/49%).

As indicated above, compound **2** is poorly soluble in the reaction media (at least 78 wt % of the initial amount of solid could be recovered by centrifugation when no cosolvent was used, compared with at least 88 wt % when either *n*-hexane or DCE was used). The natures of the catalytic reactions (homogeneous and/or heterogeneous) were investigated by performing the CatFilt experiment (as described in the Experimental Section) for **2** and comparing the results (i.e., the increase in conversion between 1 and 24 h, denoted as $\Delta X(\text{CatFilt})$ with those obtained for the same reaction in the presence of **2** ($\Delta X(\text{NoFilt})$) or in the absence of a catalyst ($\Delta X(\text{NoCat})$). The values of $\Delta X(\text{NoFilt})$, $\Delta X(\text{CatFilt})$, and $\Delta X(\text{NoCat})$ were 32%, 23%, and 5% for no cosolvent; 39%, 13%, and 6% for DCE; and 21%, 10%, and 10% for *n*-hexane. The fraction $\Delta X(\text{CatFilt})/\Delta X(\text{NoCat})$ decreases in the order no cosolvent (5.7) > DCE (2.3) > *n*-hexane (1.0), which indicates that the contribution from the homogeneous phase reaction is more significant for no cosolvent than for DCE, and negligible for *n*-hexane. The extent to which molybdenum-containing active species dissolve at the beginning of the reaction is influenced by the solvent, being enhanced in more polar media. As discussed ahead, the characterization

(36) Bernstein, J.; Davis, R. E.; Shimoni, L.; Chang, N. L. *Angew. Chem., Int. Ed. Engl.* **1995**, *34*, 1555.

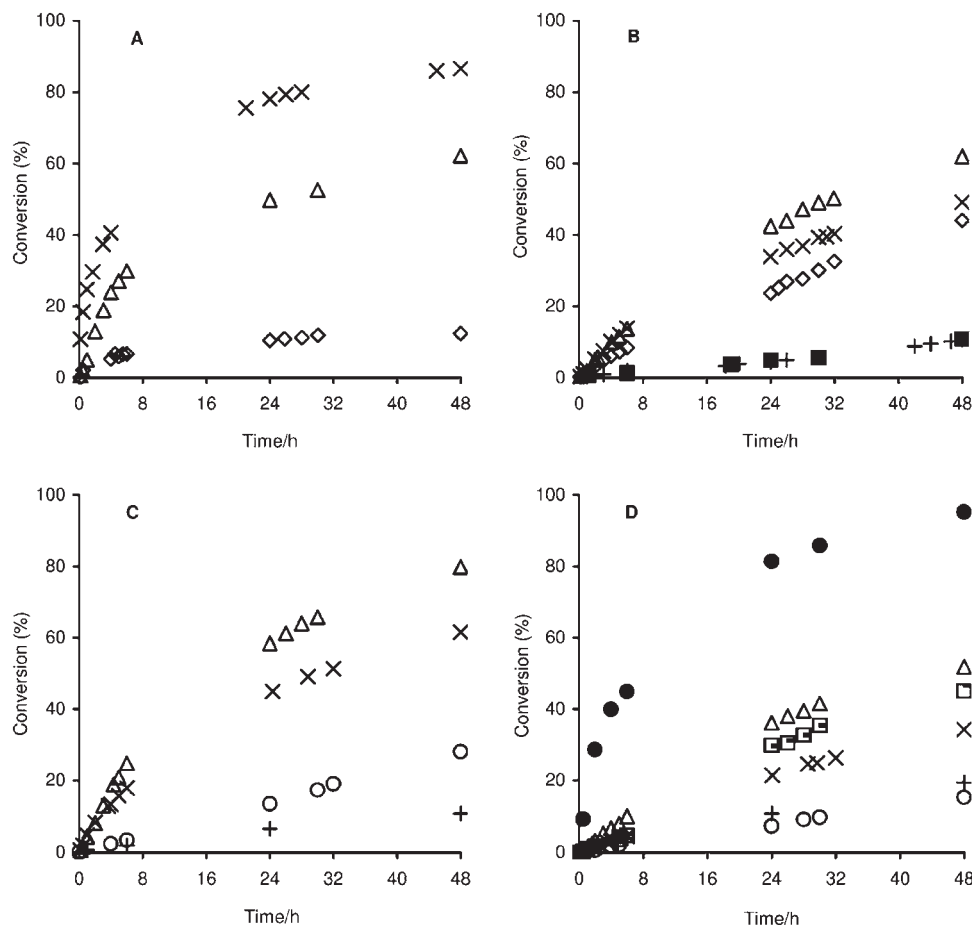


Figure 6. Epoxidation of *cis*-cyclooctene at 55 °C (unless otherwise stated) using **1** and no additional cosolvent (A), **2** and no additional cosolvent (B), **2** and 1,2-dichloroethane (C), and **2** and *n*-hexane (D). The reactions carried out with *t*BuOOH(decane) as the oxidant are as follows: run 1 with catalyst [55 °C (×) or 75 °C (●)], runs with recovered catalyst [run 2 (Δ), run 3 (—), run 4 (□)], liquid phase recovered after run 1 (○), without catalyst (+). Catalytic runs using aqueous *t*BuOOH (◇) or aqueous H₂O₂ (■) instead of *t*BuOOH(decane) are also shown.

results for the as-prepared and recovered catalysts are similar, and thus it is possible that the homogeneous contribution is due to the dissolution of a fraction of **2** rather than to its decomposition into soluble, active metal species. Polar reaction media may enhance the solubility of **2** by disrupting the O—H···O hydrogen bonding between the interconnected chains.

After the normal (i.e., unfiltered) catalytic runs at 55 °C with **2** and either *n*-hexane or DCE as a cosolvent, the reaction mixtures were centrifuged at 48 h to separate the solids from the reaction solutions, and fresh olefin and oxidant were added (in similar amounts to those used in the first run) to the solutions, which were heated for a further 48 h at 55 °C. As shown in Figure 6, the reaction in the homogeneous phase with *n*-hexane was actually slower than that observed without a catalyst (possibly due to dilution effects). An AAS analysis of the reaction solution for *n*-hexane (after separating the solid) revealed no measurable amount of molybdenum (less than 1 ppm). These results are consistent with the CatFilt results and confirm that the catalytic reaction with **2** is essentially heterogeneous in nature when *n*-hexane is employed as a cosolvent. Conversely, the same experiment performed for DCE shows that the solution contained active species, giving a 14%/28% epoxide yield with a 24 h/48 h reaction, whereas without a catalyst, the epoxide yields were 7%/11%. With *n*-hexane the reaction in the presence or

absence of **2** gives comparable epoxide yields up to ca. 6 h, and afterward the reaction is faster in the presence of a catalyst. The observed induction period for the catalytic reaction may be partly due to diffusion limitations.

The stability and reusability of **2** were further investigated by recovering the solid (as described in the Experimental Section) at 48 h for each reaction and reusing it in a second reaction run. For each system studied, the epoxide yields for runs 1 and 2 are similar during an initial period of time (ca. the first 6 h for no cosolvent, the first 2 h for DCE, and the first 30 min for *n*-hexane), and afterward the yields are higher in the second run (Figure 6). A further two runs were carried out in the case of *n*-hexane; the kinetic curves for the third and fourth runs are roughly coincident and lie between those for runs 1 and 2 (Figure 6D). After each of the second 48 h runs, the solids were recovered by filtration and washed and dried, and ATR FT-IR spectra were measured and compared with that for **2**. Figure 2 shows representative spectra for **2** and the solid recovered after the second catalytic run of 48 h without cosolvent. All of the spectra were very similar in the range of 300–1750 cm⁻¹, suggesting that the recovered solids were structurally very similar to as-prepared **2**. This was supported by obtaining CHN microanalyses for the solid recovered after the second run carried out without cosolvent, which were found to be comparable with those obtained for as-prepared **2**. The powder XRD patterns

for as-prepared **2** and the solid recovered after the first run carried out using *n*-hexane were practically identical (Figure S1 in the Supporting Information). Hence, these data do not provide any evidence to suggest that the solid phase undergoes significant structural modifications during the catalytic reactions. Further studies are underway to clarify the causes of the observed differences in catalytic activity between runs.

With *n*-hexane as the cosolvent, the catalytic activity is considerably improved by increasing the reaction temperature from 55 to 75 °C: conversion at 24 h/48 h is 22%/34% at 55 °C and 81%/95% at 75 °C (Figure 6D). The CatFilt experiment performed at 75 °C (with catalyst filtration at 30 min and leaving the reaction solution to react for a further 5.5 h) gave $\Delta X(\text{CatFilt}) = 9\%$ compared to $\Delta X(\text{NoFilt}) = 36\%$, and a $\Delta X(\text{CatFilt})/\Delta X(\text{NoCat})$ of *ca.* 1, indicating that the reaction takes place essentially in the heterogeneous phase.

As found for compound **2**, the reaction of Cy8 with *t*BuOOH (5.5 M in decane) in the presence of **1**, at 55 °C, is a biphasic solid–liquid (without a cosolvent), and the solid recovered after the first 48 h run shown in Figure 6 corresponded to about 56 wt % of the initial amount of **1** used. The recovered solid was used in a second 48 h run (Figure 6). After the first 10 min, the reaction is slower in run 2 than in run 1 (epoxide yields at 24 h/48 h are 78%/87% and 50%/62% for runs 1 and 2, respectively), in contrast to that observed for **2**. The ATR FT-IR spectra of the solids recovered after the first and second runs were similar, but different from that exhibited by **1**, especially in the region of 300–1000 cm^{-1} (Figure 2). Thus, the strong bands at 340 ($\nu(\text{Mo}-\text{Cl}_{\text{asym}})$), 904 ($\nu(\text{Mo}=\text{O}_{\text{asym}})$), and 935 cm^{-1} ($\nu(\text{Mo}=\text{O}_{\text{sym}})$) for **1** are replaced by bands at 317, 355, 871 (sh), 881, and 913 cm^{-1} for the recovered solids, and a very intense, broad absorption appears around 615 cm^{-1} . In fact, the spectra for the recovered solids (Figure 2f) are remarkably similar to that exhibited by the hybrid polymer $[\text{MoO}_3(\text{bipy})]$ (Figure 2e).¹⁴ The catalytic reaction with **1** was scaled up 10 times (i.e., 0.18 mmol of **1**) and carried out in a round bottomed flask. After 24 h, the solid was isolated by filtration, washed with *n*-hexane and diethyl ether, and vacuum-dried. The elemental analysis (CHN) and FT-IR data for this solid matched those expected for $[\text{MoO}_3(\text{bipy})]$. The yield was 40 mg (74%). The transformation of **1** into $[\text{MoO}_3(\text{bipy})]$ under the catalytic reaction conditions probably occurs due to the presence of small amounts of water (the supplied *t*BuOOH solution was used as received and may contain up to 4% water), resulting in hydrolysis of the Mo–Cl bonds.

The catalytic performances of **1** and **2** were further studied using 70% aqueous *t*BuOOH or 30% aqueous H_2O_2 instead of *t*BuOOH(decane). Triphasic solid–organic–aqueous mixtures were formed. For both compounds, when aqueous *t*BuOOH was used, the reactions were either slower (**2**) or much slower (**1**) than those performed using *t*BuOOH(decane) (Figure 6), although selectivity to the epoxide was always 100%. These results may be partly due to the fact that at least the oxidant is partitioned between the aqueous and organic phases, and mass transfer limitations may exist. The ATR FT-IR spectra of the recovered solids were similar to that for

as-prepared **2** (compare Figure 2a with c and g), which suggests that **1** transforms into **2** under the catalytic reaction conditions (i.e., in the presence of excess water), and that **2** is fairly water tolerant. With aqueous H_2O_2 and compound **2**, the resultant kinetic curve was nearly coincident with that observed for the reaction of Cy8 with *t*BuOOH(decane) in the absence of a catalyst (Figure 6). The sluggish reaction may be due to the inability of the catalyst to activate H_2O_2 for oxygen atom transfer to the olefin.

Concluding Remarks

The chemistry of Mo^{VI} continues to be a topic of great interest. One of the main driving forces for ongoing synthetic efforts is to find better catalysts for the epoxidation of olefins. Most reactions are carried out in organic solvents using *tert*-butylhydroperoxide as the oxidant, but the use of aqueous media is gaining interest. The chemistry of well established Mo^{VI} epoxidation catalysts in water is therefore worth studying. In the present work, we expected that the reaction of the complex $[\text{MoO}_2\text{Cl}_2(\text{bipy})]$ in water could lead to the organic–inorganic hybrid material $[\text{MoO}_3(\text{bipy})]$, which was recently shown to be an active, highly selective, and stable catalyst for the epoxidation of *cis*-cyclooctene with *t*BuOOH. However, regardless of the heating method used, the hydrolysis reaction actually gives high yields of the hybrid material $\{[\text{MoO}_3(\text{bipy})][\text{MoO}_3(\text{H}_2\text{O})]\}_n$ (**2**), which has an unprecedented structure formed by the 1:1 adduct of one-dimensional inorganic and organic–inorganic polymers. The catalytic tests show that **2** is a moderately active, highly selective, and stable catalyst for the epoxidation of *cis*-cyclooctene at 55 °C with *t*BuOOH (in decane) as the oxidant. The catalysis is heterogeneous in nature when *n*-hexane is used as a cosolvent. When the catalytic reaction is carried out using the precursor **1**, the hybrid material $[\text{MoO}_3(\text{bipy})]$ is formed, presumably due to the presence of residual water. On the other hand, with 70% aqueous *t*BuOOH, compound **2** is isolated at the end of the catalytic run. Furthermore, the selective epoxidation of the olefin can be performed using **2** and aqueous *t*BuOOH.

We conclude that hybrid molybdenum oxide-based materials like $[\text{MoO}_3(\text{bipy})]$ and $\{[\text{MoO}_3(\text{bipy})][\text{MoO}_3(\text{H}_2\text{O})]\}_n$ comprise potentially interesting water tolerant catalysts for the epoxidation of nonfunctionalized olefins. Ongoing work in our laboratories is focused on investigating the chemistry of other complexes of the type $[\text{MoO}_2\text{X}_m\text{L}_n]$ in water, which may provide a series of novel materials with different structures and catalytic properties.

Acknowledgment. The authors are grateful to the Portuguese Science Foundation (FCT), POCI 2010, OE, and FEDER for funding through the projects PTDC/QUI/65427/2006, PTDC/QUI/71198/2006, and PTDC/QUI-QUI/098098/2008. M.M.A. and S.G. thank the FCT for Ph.D. and postdoctoral grants, respectively. We acknowledge the European Synchrotron Radiation Facility (Grenoble, France) for granting access time to the ID31 beamline.

Supporting Information Available: Crystallographic information file (CIF) for compound **2** and powder XRD patterns for as-prepared **2** and recovered catalyst. This material is available free of charge via the Internet at <http://pubs.acs.org>.